OPEN

The intrinsic disorder related alloy scattering in ZrNiSn half-Heusler thermoelectric materials

Hanhui Xie[1], Heng Wang[2], Chenguang Fu[1], Yintu Liu[1], G. Jeffrey Snyder[2], Xinbing Zhao[1] & Tiejun Zhu[1,3]

[1]State Key Laboratory of Silicon Materials, Department of Materials Science and Engineering, Zhejiang University, Hangzhou 310027, China, [2]Department of Materials Science, California Institute of Technology, Pasadena, CA 91125, (USA), [3]Cyrus Tang Center for Sensor Materials and Applications, Zhejiang University, Hangzhou, 310027, China.

The intrinsic structural disorder dramatically affects the thermal and electronic transport in semiconductors. Although normally considered an ordered compound, the half-Heusler ZrNiSn displays many transport characteristics of a disordered alloy. Similar to the (Zr,Hf)NiSn based solid solutions, the unsubstituted ZrNiSn compound also exhibits charge transport dominated by alloy scattering, as demonstrated in this work. The unexpected charge transport, even in ZrNiSn which is normally considered fully ordered, can be explained by the Ni partially filling interstitial sites in this half-Heusler system. The influence of the disordering and defects in crystal structure on the electron transport process has also been quantitatively analyzed in $ZrNiSn_{1-x}Sb_x$ with carrier concentration n_H ranging from 5.0×10^{19} to 2.3×10^{21} cm^{-3} by changing Sb dopant content. The optimized carrier concentration $n_H \approx 3-4 \times 10^{20}$ cm^{-2} results in $ZT \approx 0.8$ at 875K. This work suggests that MNiSn ($M =$ Hf, Zr, Ti) and perhaps most other half-Heusler thermoelectric materials should be considered highly disordered especially when trying to understand the electronic and phonon structure and transport features.

T hermoelectric (TE) materials, which offer the possibility of directly converting waste heat into usable electricity, could be an important part of the solution to today's energy crisis[1]. The efficiency of a TE material is represented by the dimensionless figure of merit $ZT = S^2\sigma T/\kappa$, where S is the Seebeck coefficient, σ is the electrical conductivity, T is the operating temperature and κ is the total thermal conductivity arising from two prime contributions, namely, the lattice part κ_L and the electronic part κ_e. An in-depth understanding of electron and phonon transport in typical TE materials has led to fruitful strategies based on optimizing the tunable transport parameters[2]. Two approaches have been adopted to improve the efficiency of thermoelectrics: increase the power factor $S^2\sigma$ by engineering the electronic structure, and reduce κ_L by introducing additional phonon scattering without the deterioration of power factor. For example, band convergence[2,3], resonant states from impurity doping[4,5], and nanostructuring[6,7] have been demonstrated to be effective in achieving high ZT for various TE systems.

The TE quality factor $B \propto \mu m^{*\frac{3}{2}}/\kappa_L$[8], which is proportional to the density-of-states (DOS) effective mass m^*, the carrier mobility μ, and the reciprocal lattice thermal conductivity κ_L, determines the optimal ZT of thermo-electrics presuming the dominant scattering mechanism is known. The mobility is sensitive to the effective mass and scattering mechanisms. While a large m^* is favourable for high S, it will possibly lead to a significant reduction in mobility[9]. Acoustic phonon scattering, which gives a $\mu \propto T^{-3/2}$ dependence, is demonstrated to be the dominant carrier scattering mechanism in most of TE materials used above room temperature with the absence of bipolar effects[10,11]. In solid solutions, the atomic level disorder causes local potential energy fluctuations that induce additional carrier scattering, that is, disorder scattering or alloy scattering with a $\mu \propto T^{-1/2}$ relationship. Such a scattering was first studied in metal alloys[12] and found having significant influences on the transport behaviour in some TE alloys[13–15]. For systems in which the optical phonon branches are prevalent, polar scattering from optical phonons, which also follows $\mu \propto T^{-1/2}$ dependence, can be prominent at low carrier concentrations[16]. Scattering by neutral or ionized impurities, dislocations and grain boundaries are generally weak in magnitude in dense semiconducting samples, and in most cases, are only noticeable at low temperatures.

Half-Heusler (HH) alloys, with a valence electron count of 18, have been extensively studied as potential high temperature TE materials due to their narrow band gap and sharp slope of the density of states near the Fermi level[17–20]. Among them, the HH compounds of the general formula MNiSn ($M =$ Ti, Hf, Zr) have been of
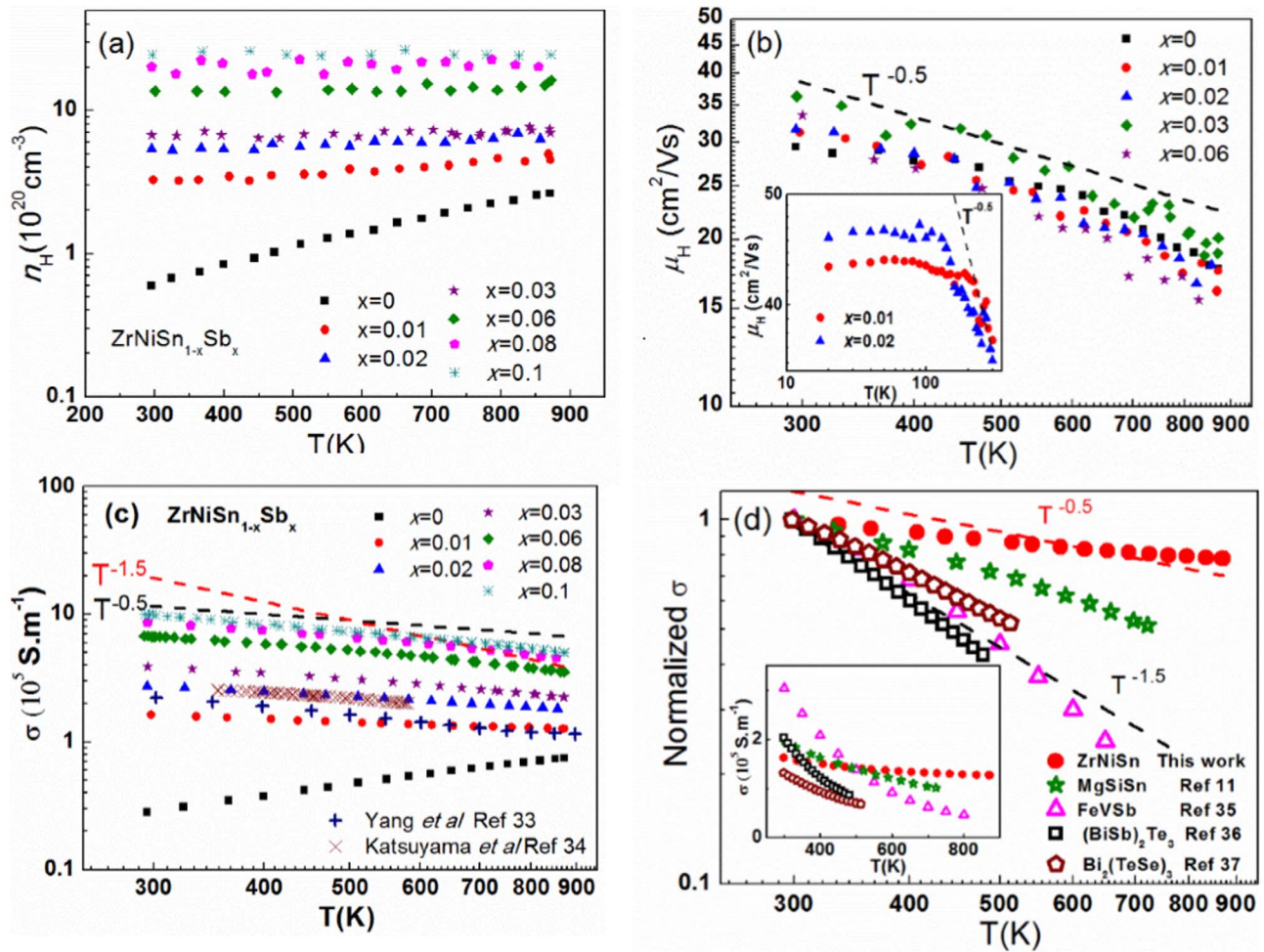
Figure 1 | Temperature dependences of (a) carrier concentration n_H, (b) Hall mobility μ_H (The inset shows the low temperature Hall mobility.), and (c) electrical conductivity for $ZrNiSn_{1-x}Sb_x$ ($x = 0$–0.1) samples. (d) Normalized electrical conductivity of $ZrNiSn_{0.99}Sb_{0.01}$, compared to other TE materials. (The inset shows the electrical conductivity as a function of temperature.)

significant interest for their high power factors ($S^2\sigma$) due to the combination of large Seebeck coefficient ($S \approx 200$ µV K^{-1} at room temperature) and reasonably high electrical conductivity ($\sigma \approx 10^4$ S m^{-1} at room temperature). Many efforts have been devoted to tune the carrier concentration by doping Sb on Sn sites[17,21], or to control the atomic antisite disorder[22]. However, the high thermal conductivity makes this system less promising for TE applications. To reduce the lattice thermal conductivity, the effectiveness of isoelectronic alloying on the M or Ni sublattice in causing additional mass or strain fluctuation[17,23,24], or grain refinement in enhancing phonon scattering at boundaries[25,26], have been demonstrated.

While the TE performance of MNiSn alloys has been significantly optimized and a maximum $ZT \sim 1$ has been obtained at 1000 K for Hf$_{0.6}$Zr$_{0.4}$NiSn$_{0.98}$Sb$_{0.02}$ composition[21], there are few analyses on the electron and phonon transport characteristics. ZrNiSn is predicted to have an indirect band gap, and the conduction band extrema is located at the X point of the Brillouin zone[27–29]. Recently, we have
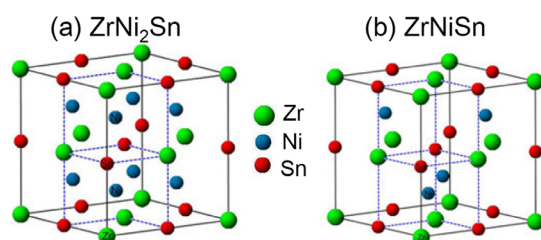
Figure 2 | The crystal structure of (a) Heusler ZrNi$_2$Sn system and (b) half-Heusler ZrNiSn system. The octahedral sites formed by Zr-Sn are half occupied in the half-Heusler system.
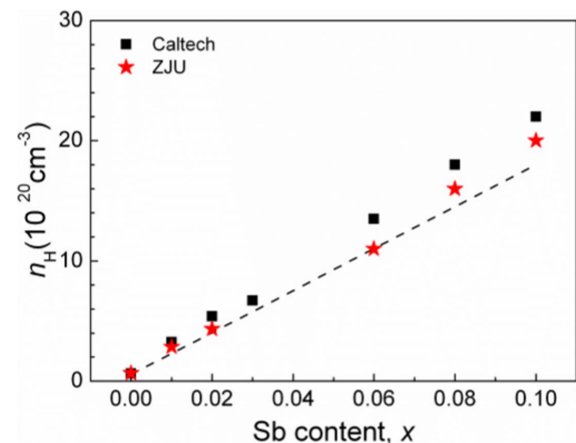
Figure 3 | Room temperature Hall carrier density as a function of Sb content. The experimental carrier density is slightly higher than the calculated values, assuming each Sb atom provides exactly one electron for ZrNiSn$_{1-x}$Sb$_x$ system (dashed line).
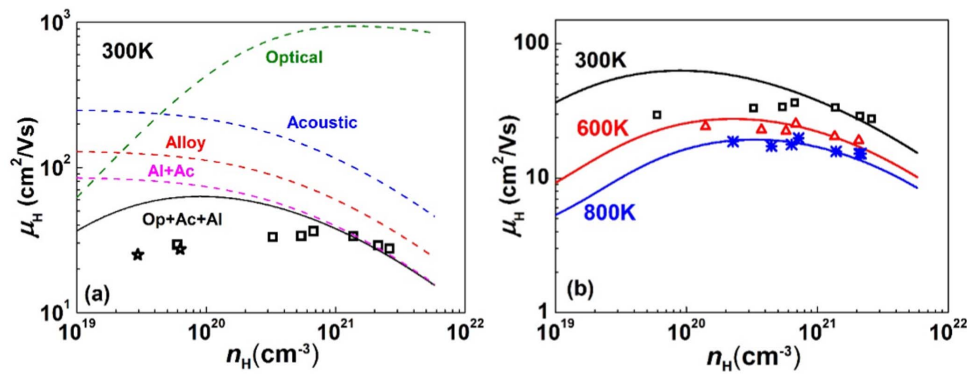
Figure 4 | (a) Hall mobility as a function of Hall carrier density at 300 K for ZrNiSn$_{1-x}$Sb$_x$ ($x = 0$–0.1). (b) Hall mobility as a function of Hall carrier density for ZrNiSn$_{1-x}$Sb$_x$ ($x = 0$–0.1) at 300 K, 600 K and 800 K. The solid curves are calculated taking into account polar, alloy and acoustic phonon scattering. The dashed lines show the calculated contribution of individual scattering mechanism.

analyzed the transport properties of n-type (Zr,Hf)NiSn based solid solutions by the single parabolic band (SPB) model[30]. A low deformation potential E_{def}, describing the coupling between phonons and electrons, and a low alloy scattering potential E_{al}, characterizing the strength of local potential energy fluctuation caused by substitution atoms, are found to be beneficial for maintaining a relatively high electron mobility despite of the large DOS effective mass ($m^* = 2.8 \pm 0.2\ m_e$). These are intrinsically favourable features contributing to the noticeably high power factors of ZrNiSn based alloys[30]. However, when the energy of an electron is comparable with the energy gap (E_g), the dependence of energy on the crystal momentum is often nonquadratic[31], which may lead to a deviation from the SPB model. In this case, the single Kane band (SKB) model, which takes into account the first order nonparabolicity and provides a more accurate description of the electrical transport properties, should be used, as demonstrated in PbTe and PbSe systems[2,9,10,31,32].

In addition, different from most of high performance TE materials with dominant acoustic phonon scattering[10,11,31], the heavily substituted ZrNiSn (Hf at Zr sites and Pt at Ni sites) alloys exhibits a charge transport dominated by alloy scattering as observed by the $\mu_H \sim T^{-1/2}$ dependence[30]. In order to deeply probe into the charge transport mechanisms in ZrNiSn based HH alloys, the TE transport characteristics of unsubstituted ZrNiSn alloys should be studied.

In this paper, we study the TE transport of n-type ZrNiSn alloys with no substitutions at Zr or Ni sites but with a small amount of Sb dopant (with similar size and electronic structure as Sn) to adjust the carrier concentration, in order to gain insight understanding of TE transport features in this compound. The experimental electrical properties are analyzed by the SKB model. Surprisingly, the unsubstituted ZrNiSn alloys also exhibit an alloy scattering dominated electron transport, even in the lightest doped samples, which is ascribed to the atomic disorder caused by the fractional occupancy of interstitial sites by Ni in this system. This result demonstrates the significance of intrinsic point defect disorder in affecting the charge transport in TE materials.

Results and Discussion

The XRD patterns of all the ZrNiSn$_{1-x}$Sb$_x$ ($x = 0$-0.1) samples are easily indexed to the cubic MgAgAs-type HH crystal structure (Fig. S1, Supplementary Information). Figure 1(a) shows that the n-type Hall carrier density can be tuned from 5.0×10^{19} to 2.3×10^{21} cm^{-3} by changing Sb content. The n_H obtained is roughly independent of temperature in the measured temperature range except for the undoped sample, of which the n_H increases with temperature, indicating the existence of impurity states or the excitation of minority carriers. Surprisingly, the Hall mobility μ_H of the ZrNiSn samples in
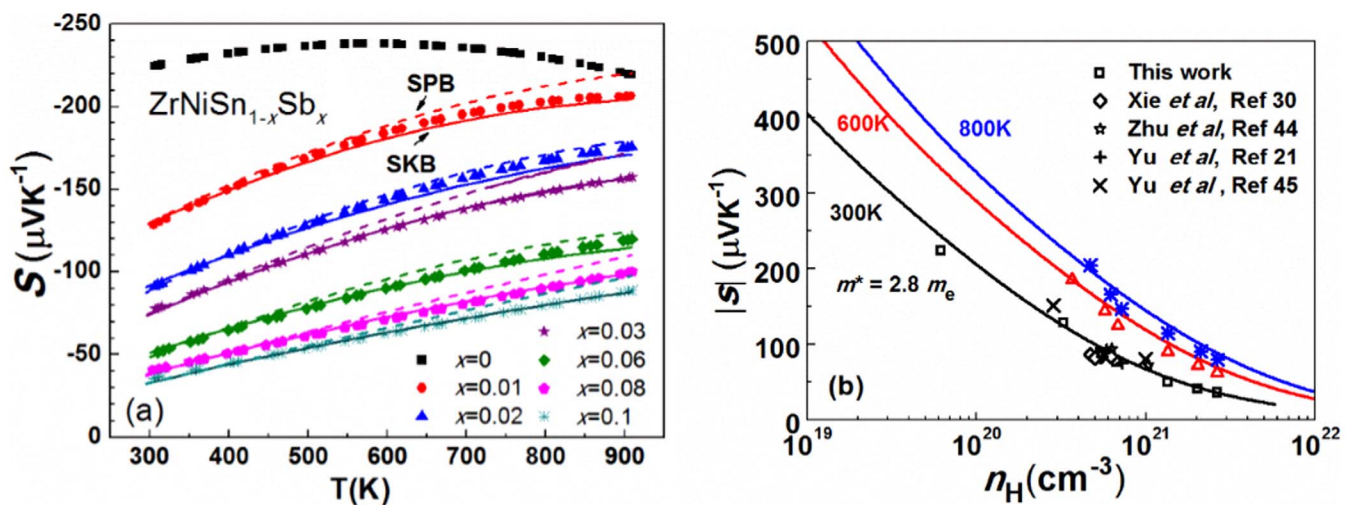
Figure 5 | (a) Seebeck coefficient as a function of temperature for ZrNiSn$_{1-x}$Sb$_x$ ($x = 0$–0.1) samples. The solid curves are performed based on SKB model while the dashed curves are calculated on SPB model. (b) Seebeck coefficient as a function of Hall carrier density. The solid curves are calculated taking into account polar, alloy and acoustic phonon scattering. The Pisarenko curves based on each mechanism are presented in the Supplementary Information.
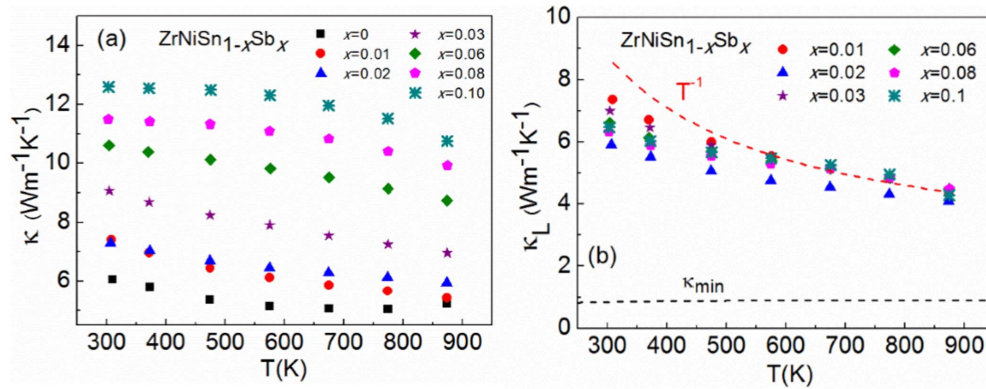
Figure 6 | (a) The temperature dependence of thermal conductivity and (b) lattice thermal conductivity for $ZrNiSn_{1-x}Sb_x$ (x = 0–0.1) samples.

Figure 1(b) follows a temperature dependence of $T^{-0.5}$, implying an alloy scattering dominated carrier scattering mechanism. Figure 1(c) shows that all doped samples ($x \geq 0.01$) exhibit a degenerate semiconductor behavior, with the electrical conductivity decreasing with temperature. A typical alloy scattering behavior $\sigma \sim T^{-0.5}$ was again observed, consistent with the trend of σ for unsubstituted ZrNiSn compounds reported by other groups[33,34]. The temperature dependence of normalized electrical conductivity of ZrNiSn, together with other TE materials[11,35–37], is shown in Figure 1(d). Different from those systems with charge transport dominated by acoustic phonon scattering, displaying $\sigma \sim T^{-1.5}$ dependence, the unsubstituted ZrNiSn compounds obviously exhibits a lower decay rate of σ, due to a different carrier scattering mechanism.

It is astonishing that the unsubstituted ZrNiSn alloys exhibit an alloy scattering dominated charge transport, which should not result from the Sb doping alone because Sb has the similar atomic radius to Sn and the Sb content is small. The unexpected alloy scattering should be related to the intrinsic atomic disorder in ZrNiSn alloys. The crystal structures of half-Heusler compound ZrNiSn and Heusler alloy $ZrNi_2Sn$ are given in Figure 2. A distinct feature of crystal structure of ZrNiSn in comparison with $ZrNi_2Sn$ is the presence of un-occupied interstitial sites in each unit cell[38]. It is reported that there may exist Ni/interstitial site or Zr/Sn antisite disorder in ZrNiSn[38,39]. The atomic radii of Zr (0.160 nm) and Sn (0.158 nm) are similar[38] such that antisite defects were claimed to be responsible for the electrical conductivity change before and after annealing in arc-melted ZrNiSn samples[17,22]. The crystallographic order of HH alloys is sensitive to the preparation method[17,22,39]. For the levitation-melted ZrNiSn samples, no Zr/Sn antisite defects were observed but a fractional occupancy of Ni on the interstitial site (1/2, 1/2, 1/2) was implied by the Fourier charge density map, and was further confirmed by Rietveld refinements based on high-resolution synchrotron radiation powder X-ray diffraction results[39]. Band structure

calculation reveals that the formation energy of Zr/Sn antisite disorder is higher than that of Ni/interstitial disorder[40]. The electronic structure of MNiSn(M = Hf, Zr, Ti) HH alloys was also experimentally studied by photoemission spectroscopy excited by soft and hard X-ray synchrotron radiation, and the in-gap electronic states were observed due to the existence of two Ni atoms with different electron occupancies, implying the existence of Ni/interstitial disorder[41].

Figure 3 shows that the measured Hall carrier concentrations are a little higher than those calculated assuming that each Sb atom provides exactly one electron for $ZrNiSn_{1-x}Sb_x$ according to the simple valence principle[42]. The increased Hall carrier concentrations at high Sb contents could be due to the influence of the intrinsic point defects in this system. The EPMA results (Table S1) revealed about 5% excess of Ni in the $ZrNiSn_{1-x}Sb_x$ samples, which may occupy the interstitial sites, as previously observed in ZrNiSn samples[39]. The excess Ni can act as electron donors[43], and result in an increase in carrier concentration.

The SKB model is used to analyze the electrical transport of the ZrNiSn samples (see Supplementary Information). Although the alloy scattering due to the point defect disorder is dominant, the acoustic phonon scattering and the polar scattering are also taken into account. Acoustic phonon scattering, or more precisely deformation potential scattering due to non-polar scattering of acoustic and optical phonons[10], often dominates charge transport of TE materials. ZrNiSn system is also a polar semiconductor and may have a certain degree of polar scattering from optical phonons.

With the total carrier relaxation time determined by Matthiessen's rule $\tau_{total}^{-1} = \tau_{ac}^{-1} + \tau_{po}^{-1} + \tau_{alloy}^{-1}$ (τ_{total} is defined as the total relaxation time, while τ_{ac}, τ_{po} and τ_{alloy} are the relaxation times caused by acoustic phonon, polar and alloy scattering, respectively. More details in Supplementary Information), the electrical transport properties of the ZrNiSn samples can be quantitatively calculated by the
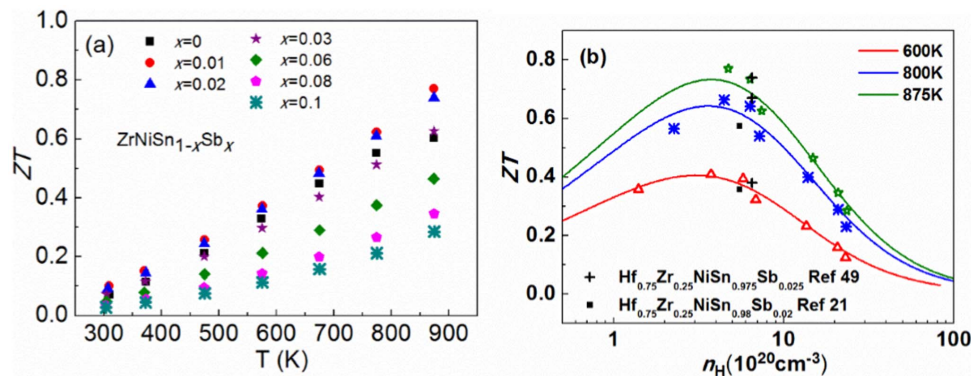
Figure 7 | (a) ZT as a function of temperature and (b) ZT as a function of Hall carrier concentration for Sb doped for $ZrNiSn_{1-x}Sb_x$ (x = 0–0.1).

SKB model throughout the temperature range discussed in this paper.

Figure 4(a) shows that alloy scattering makes the dominant contribution to the charge transport at 300 K in ZrNiSn alloys, and the calculated mobilities involving both the alloy scattering and acoustic phonon scattering can match well with the experimental mobilities at high carrier concentrations ($>10^{21}$ cm^{-3}). The influence of the polar optical phonon scattering on μ becomes notable in the low carrier concentration range. With increasing temperature, the calculated carrier concentration dependence of mobility by the SKB model agrees well with the experimental Hall mobility within the n_H range from 5.0×10^{19} to 2.0×10^{21} cm^{-3}, as displayed in Figure 4(b). The small amount (~5%) of atomic disorder in ZrNiSn alloys is apparently sufficient to result in an alloy scattering dominated electron transport, implying the significance of intrinsic point defect disorder in affecting the charge transport in TE materials.

Figure 5(a) shows the temperature dependence of the Seebeck coefficient for ZrNiSn$_{1-x}$Sb$_x$ ($x = 0$–0.1). S decreases with Sb content due to the increased carrier concentration. The calculated Seebeck coefficients, based on the SKB model with the DOS effective mass $m^* = 2.8\,m_e$ (solid curves), agree well with the experimental data in the measured temperature range, while the curves calculated by the SPB model (dash curves) show a deviation from the experimental points above 500 K, indicating that the interaction of conduction band and valance band is more prominent in charge transport at high temperatures and there the SKB model may be more accurate. The calculated Pisarenko curves at different temperatures by the SKB model, with effective mass $m^* = 2.8 \pm 0.1\,m_e$ at several temperatures, as displayed in Figure 5(b), agree well with the measured n_H dependence of S together with the literature data[21,30,44,45]. Note that with increasing temperature, the DOS effective mass slightly decreases from $m^* = 2.8\,m_e$ at 300 K to $m^* = 2.7\,m_e$ at 800 K. Although the slight difference looks to be within the data noise and the fit quality, we should bear in mind that the decreasing m^* with temperature can also contribute to the temperature dependence of mobility and makes it flatter. The more accurate determination of m^* will be beneficial to clarify its contribution to $\mu \sim T^{-0.5}$ dependence observed in this work.

The thermal conductivity decreases with temperature for all the doped samples and the bipolar contribution was observed above 600 K for the undoped sample as shown in Figure 6(a). The electronic thermal conductivity was calculated by the Wiedemann-Franz law using the Lorenz number based on the SKB model (in Supplementary Information). It can be seen from Figure 6(b) that the experimental data follows the $\kappa_L \sim T^{-1}$ at high temperatures since the Umklapp process becomes more prominent with temperature, while a small deviation from $\kappa_L \sim T^{-1}$ around room temperature was observed, which can be expected from the influence of intrinsic point defect scattering due to the fractional occupancy of interstitial sites by Ni in this system. The observed temperature dependence of κ_L can be understood as a sum of contributions mainly from the Umklapp scattering of acoustic phonons with T^{-1} dependence[46] and alloy scattering with $T^{-0.5}$ dependence[47]. The κ_L up to 875 K is well above the minimum thermal conductivity of this system predicted with the Cahill model[48].

A maximum ZT of 0.8 was achieved at 875 K for the ZrNiSn$_{0.99}$Sb$_{0.01}$ sample, as shown in Figure 7(a), which is comparable to the isoelectronic alloyed MNiSn ($M = $ Hf, Zr, Ti) compounds[21,49]. Since the Seebeck coefficient in this system is highly sensitive to the carrier density, over-doping, as observed in our previous work ($n_H \approx 6$–7×10^{20} cm^{-3})[21], has resulted in the deterioration of the TE performance. Even higher ZT could be achieved in this work if the measurement were extended to higher temperatures, since the Seebeck coefficient is still increasing and the contribution of bipolar effect is not prominent at 875 K. The theoretical figure of merit $ZT = S^2 \sigma T / \kappa$ was calculated based on the SKB model, as shown

in Figure 7(b). The theoretical curve at 875 K was calculated assuming minority carriers have no significant influence on the electron transport. The maximum ZT and corresponding optimum Hall carrier density increase with increasing temperature. Both experimental work and theoretical calculations show that the optimal carrier concentrations are near $n_H \approx 3$–4×10^{20} cm^{-3}.

Conclusions

Similar to heavily substituted (Zr,Hf)NiSn based solid solution alloys, the unsubstituted ZrNiSn compounds also exhibit an alloy scattering dominated charge transport, as demonstrated by a $\mu_H \sim T^{-0.5}$ dependence. The unexpected transport phenomenon can be explained by the Ni partially filling interstitial sites. The analyses revealed that even the small amount of atomic disorder in ZrNiSn half-Heusler alloys is apparently sufficient to result in an alloy scattering dominated electron transport, implying the significance of intrinsic point defect disorder in affecting the charge transport in TE materials. Both experimental work and theoretical calculations show that the optimized ZT values are near $n_H \approx 3$–4×10^{20} cm^{-3}. The highest $ZT \approx 0.8$ was obtained for ZrNiSn$_{0.99}$Sb$_{0.01}$ at 875 K. This work suggested that MNiSn and perhaps most other half-Heusler thermoelectric materials should be considered disordered especially when trying to understand the electronic and phonon structure.

Methods

High quality samples were fabricated by a time-efficient method combining levitation melting and spark plasma sintering (SPS)[21]. Alloys with nominal composition ZrNiSn$_{1-x}$Sb$_x$ ($x = 0, 0.01, 0.02, 0.03, 0.06, 0.08, 0.1$) were first prepared by levitation melting of stoichiometric amounts of Zr (piece, 99.99%), Ni (block, 99.99%), Sn (particles, 99.99%), and Sb (block, 99.99%) under an argon atmosphere for 2 min, and the melt was quenched in a water-cooled copper crucible. The ingots were remelted twice to ensure homogeneity. Mechanical milling was carried out in Retsch MM200 Mill with an oscillation frequency of 20 Hz for 20 min. The powders were then sintered by SPS (SPS-1050, Sumitomo Coal Mining Co.) at 1175 K under 65 MPa in vacuum for 10 min. The as-sintered samples, of which the relative densities were ~95%, were used for the thermal conductivity, electrical conductivity and Hall measurements, and then cut into rectangular bars for Seebeck coefficient measurement.

The phase structure of powders and sintered samples were studied by X-ray diffraction (XRD) on a RigakuD/MAX-2550PC diffractometer using Cu Ka radiation ($\lambda = 1.5406$ Å), and the chemical composition was analyzed by electron probe microanalysis (EPMA, JOEL, JXA-8100) using wavelength dispersive spectroscopy (WDS).

The in-plane electrical conductivity and Hall coefficients were measured using the Van der Pauw method in a magnetic field up to ± 2 T[50]. The Hall carrier concentration n_H was calculated via $n_H = 1/eR_H$, where R_H is the Hall coefficient and e is the electron charge. The Hall mobility μ_H was calculated from the Hall coefficient and electrical conductivity $\mu_H = R_H \sigma$. The Seebeck coefficient from 300–900 K were measured on a commercial Linseis LSR-3 system using a differential voltage/temperature technique. The thermal conductivity, κ was calculated by $\kappa = D\rho C_p$, where κ is the sample density estimated by an Archimedes' method. The thermal diffusivity D, and specific heat C_p, were measured by a laser flash method on Netzsch LFA457 instrument with a Pyroceram standard. (Fig. S2, Supplementary Information). Normal and shear ultrasonic measurements were performed at room temperature using input from a Panametrics 5052 pulser/receiver with the filter at 0.03 MHz. The response was recorded via a Tektronic TDS5054B-NV digital oscilloscope.

1. Tritt, T. M. Thermoelectric materials - Holey and unholey semiconductors. *Science* **283**, 804–805 (1999).
2. Ravich, Y. I., Efimova, B. A. & Smirnov, I. A. *Semiconducting Lead Chalcogenides* [85–110] (Plenum press, New York, 1970).
3. Pei, Y. *et al.* Convergence of electronic bands for high performance bulk thermoelectrics. *Nature* **473**, 66–69 (2011).
4. Heremans, J. P., Wiendlocha, B. & Chamoire, A. M. Resonant levels in bulk thermoelectric semiconductors. *Energy Environ. Sci.* **5**, 5510–5530 (2012).
5. Heremans, J. P. *et al.* Enhancement of Thermoelectric Efficiency in PbTe by Distortion of the Electronic Density of States. *Science* **321**, 554–557 (2008).
6. Zhao, L. D. *et al.* All-scale hierarchical thermoelectrics: MgTe in PbTe facilitates valence band convergence and suppresses bipolar thermal transport for high performance. *Energy Environ. Sci.* **6**, 3346–3355 (2013).
7. Ahn, K. *et al.* Enhanced thermoelectric properties of *p*-type nanostructured PbTe–MTe (M ¼ Cd, Hg) materials. *Energy Environ. Sci.* **6**, 1529–1537 (2013).
8. Chasmar, R. P. & Stratton, R. The thermoelectric figure-of-merit and its relation to thermoelectric generators. *J. Electron. Contrl.* **7**, 52–72 (1959).

9. Pei, Y., LaLonde, A. D., Wang, H. & Snyder, G. J. Low effective mass leading to high thermoelectric performance. *Energy Environ. Sci.* **5**, 7963–7969 (2012).

10. Wang, H., Pei, Y., LaLonde, A. D. & Snyder, G. J. Weak electron–phonon coupling contributing to high thermoelectric performance in n-type PbSe. *PNAS* **109**, 9705–9709 (2012).

11. Liu, X. *et al.* Low Electron Scattering Potentials in High Performance $Mg_2Si_{0.45}Sn_{0.55}$ Based Thermoelectric Solid Solutions with Band Convergence. *Adv. Energy Mater.* **3**, 1238–1244 (2013).

12. Nordheim, L. Zur Elektronentheorie der Metalle. *Annalen der Physik*, **401**, 607–640 (1931).

13. Krishnamurthy, S., Sher, A. & Chen, A. B. Generalized Brooks Formula and the Electron-Mobility in Si_xGe_{1-x} Alloys. *Appl. Phys. Lett.* **47**, 160–162 (1985).

14. Makowski, L. & Glicksman, M. Disorder Scattering in Solid-Solutions of III-V Semiconducting Compounds. *J. Phys. Chem. Solids* **34**, 487–492 (1973).

15. Harrison, J. W. & Hauser, J. R. Alloy scattering in ternary III-V compounds. *Phys. Rev. B* **13**, 5347–5350 (1976).

16. Ravich, Y. I., Efimova, B. A. & Tamarchenko, V. I. Scattering of Current Carrier and Transport Phenomena in Lead Chalcogenides. *Phys. Stat. Sol.(b)* **43**, 11–33 (1971).

17. Uher, C., Yang, J., Hu, S. D., Morelli, T. & Meisner, G. P. Transport properties of pure and doped MNiSn (M=Zr, Hf). *Phys. Rev. B* **59**, 8615–8621 (1999).

18. Muta, H., Kanemitsu, K., Kurosaki, K. & Yamanaka, S. High-temperature thermoelectric properties of Nb-doped MNiSn (M = Ti, Zr) half-Heusler compound. *J. Alloys Compd.* **469**, 50–55 (2009).

19. Kawano, K., Kurosaki, K., Sekimoto, T., Muta, H. & Yamanaka, S. Effect of Sn doping on the thermoelectric properties of ErNiSb-based p-type half-Heusler compound. *App. Phys. Lett.* **91**, 062115 (2007).

20. Yang, J. *et al.* Evaluation of Half-Heusler Compounds as Thermoelectric Materials Based on the Calculated Electrical Transport Properties. *Adv. Funct. Mater.* **18**, 2880–2888 (2008).

21. Yu, C. *et al.* High-performance half-Heusler thermoelectric materials $Hf_{1-x}Zr_xNiSn_{1-y}Sb_y$ prepared by levitation melting and spark plasma sintering. *Acta Mater.* **57**, 2757–2764 (2009).

22. Qiu, P., Yang, J., Huang, X., Chen, X. & Chen, L. Effect of antisite defects on band structure and thermoelectric performance of ZrNiSn half-Heusler alloys. *Appl. Phys. Lett.* **96**, 152105 (2010).

23. Yan, X. *et al.* Stronger phonon scattering by larger differences in atomic mass and size in p-type half-Heuslers $Hf_{1-x}Ti_xCoSb_{0.8}Sn_{0.2}$. *Energy Environ. Sci.* **5**, 7543–7548 (2012).

24. Lee, P. J. & Chao, L. S. High-temperature thermoelectric properties of $Ti_{0.5}(Zr,Hf)_{0.5-x}Nb_xNi_{0.9}Pd_{0.1}Sn_{0.98}Sb_{0.02}$ half-Heusler alloys. *J. Alloys Compd.* **504**, 192–196 (2010).

25. Bhattacharya, S. *et al.* Effect of boundary scattering on the thermal conductivity of TiNiSn-based half-Heusler alloys. *Phys. Rev. B* **77**, 184203 (2008).

26. Bhattacharya, S. *et al.* N., Grain structure effects on the lattice thermal conductivity of Ti-based half-Heusler alloys. *Appl. Phys. Lett.* **8**, 43–45 (2002).

27. Ogut, S. & Rabe, K. M. Band-Gap and Stability in the Ternary Intermetallic Compounds NiSnM (M=Ti, Zr, Hf) - a First-Principles Study. *Phys. Rev. B* **51**, 10443–10453 (1995).

28. Ouardi, S. *et al.* Electronic transport properties of electron-and hole-doped semiconducting $C1_b$ Heusler compounds: NiTi$_{1-x}M_x$Sn (M=Sc, V). *Phys. Rev. B* **82**, 085108 (2010).

29. Chaput, L., Tobola, J., Pecheur, P. & Scherrer, H. Electronic structure and thermopower of Ni(Ti$_{0.5}$Hf$_{0.5}$)Sn and related half-Heusler phases. *Phys. Rev. B* **73**, 045121 (2006).

30. Xie, H. H. *et al.* Beneficial Contribution of Alloy Disorder to Electron and Phonon Transport in Half-Heusler Thermoelectric Materials. *Adv. Funct. Mater.* **23**, 5123–5130 (2013).

31. Pei, Y., Wang, H. & Snyder, G. J. Band Engineering of Thermoelectric Materials. *Adv. Mater.* **24**, 6125–6135 (2012).

32. Wang, H., LaLonde, A. D., Pei, Y. & Snyder, G. J. The Criteria for Beneficial Disorder in Thermoelectric Solid Solutions. *Adv. Funct. Mater.* **23**, 1586–1596 (2012).

33. Shen, Q., Yang, J. & Meisner, G. P. Effects of partial substitution of Ni by Pd on the thermoelectric properties of ZrNiSn-based half-Heusler compounds. *Appl. Phys.Lett.* **79**, 4165–4167 (2001).

34. Katsuyama, Matsuo, S. R. & Ito, M. Thermoelectric properties of half-Heusler alloys $Zr_{1-x}Y_xNiSn_{1-y}Sb_y$. *J. Alloys Compd.* **428**, 262–267 (2007).

35. Fu, C. *et al.* Electron and phonon transport in Co-doped FeV$_{0.6}$Nb$_{0.4}$Sb half-Heusler thermoelectric materials. *J. Appl. Phys.* **114**, 134905 (2013).

36. Hu, L. P. *et al.* Shifting up the optimum figure of merit of p-type bismuth telluride-based thermoelectric materials for power generation by suppressing intrinsic conduction. *NPG Asia Mater.* **6**, e88 (2014).

37. Hu, L. P. *et al.* Improving thermoelectric properties of n-type bismuth–telluride-based alloys by deformation-induced lattice defects and texture enhancement. *Acta Mater.* **60**, 4431–4437 (2012).

38. Aliev, F. G. *et al.* Metal-insulator transition of of RNiSn (R=Hf, Zr, Ti) intermetallic vacancy system. *JETP Lett.* **45**, 684–686 (1987).

39. Xie, H. H. *et al.* Interrelation between atomic switching disorder and thermoelectric properties of ZrNiSn half-Heusler compounds. *CrystEngComm* **14**, 4467–4471 (2012).

40. Larson, P., Mahanti, S. D. & Kanatzidis, M. G. Structural stability of Ni-containing half-Heusler compounds. *Phys. Rev. B* **62**, 12754–12762 (2000).

41. Miyamoto, K. *et al.* In-gap Electronic States Responsible for the Excellent Thermoelectric Properties of Ni-based Half-Heusler Alloys. *Appl. Phys. Express* **1**, 081901 (2008).

42. Toberer, E. S., May, A. F. & Snyder, G. J. Zintl chemistry for designing high efficiency thermoelectric materials. *Chem. Mater.* **22**, 624–634 (2010).

43. Romaka, V. V. *et al.* Peculiarities of structural disorder in Zr- and Hf-containing Heusler and half-Heusler stannides. *Intermetallics* **35**, 45–52 (2013).

44. Zhu, T. J. *et al.* Effects of yttrium doping on the thermoelectric properties of Hf$_{0.6}$Zr$_{0.4}$NiSn$_{0.98}$Sb$_{0.02}$ half-Heusler alloys. *J. Appl. Phys.* **108**, 044903 (2010).

45. Yu, C., Xie, H., Fu, C., Zhu, T. & Zhao, X. High performance half-Heusler thermoelectric materials with refined grains and nanoscale precipitates. *J. Mater. Res.* **27**, 2457–2465 (2012).

46. Labotz, R. J. & Mason, D. R. The Thermal Conductivity of Mg$_2$Si and Mg$_2$Ge. *J. Electrochem. Soc.* **110**, 121–126 (1963).

47. Klemens, P. G. Thermal Resistance Due to Point Defects at High Temperatures. *Phys. Rev.* **119**, 507–509 (1960).

48. Cahill, D. G., Watson, S. K. & Pohl, R. O. Lower Limit to the Thermal-Conductivity of Disordered Crystals. *Phys. Rev. B* **46**, 6131–6140 (1992).

49. Culp, S. R., Poon, S. J., Hickman, N., Tritt, T. M. & Blumm, J. Effect of substitutions on the thermoelectric figure of merit of half-Heusler phases at 800°C. *Appl. Phys. Lett.* **99**, 42106 (2006).

50. Borup, K. A. *et al.* Measurement of the Electrical Resistivity and Hall Coefficient at High Temperatures. *Rev. Sci. Instrum.* **83**, 123902 (2012).

Acknowledgments

Author contributions

H.X. wrote the main manuscript text and prepared figures 1, & 3 - 7. Y.L. prepared figure 2. H.W. and C.F. helped on the modeling. G.J.S., X.Z. and T.Z. revised the manuscript. All authors reviewed the manuscript.

Additional information

Supplementary information accompanies this paper at http://www.nature.com/scientificreports

Competing financial interests: The authors declare no competing financial interests.

How to cite this article: Xie, H. *et al.* The intrinsic disorder related alloy scattering in ZrNiSn half-Heusler thermoelectric materials. *Sci. Rep.* **4**, 6888; DOI:10.1038/srep06888 (2014).